Loss of Phase-Locking in Non-Weakly Coupled Inhibitory Networks with Finite Synaptic Decay Time

Myongkeun Oh and Victor Matveev
Department of Mathematical Sciences
and the Center for Applied Mathematics and Statistics
New Jersey Institute of Technology
Newark, NJ 07102

December 14, 2007

Abstract

The study of synchronization of coupled oscillators is important for the understanding of rhythmic activity in networks of excitable cells. Much of existing work on synchronization is centered on the weak coupling theory, which can only predict the existence of phase-locked activity. However, it is known that strong coupling can destabilize phase-locked firing in some networks. Here we show that such loss of phase-locking is a generic property of inhibitory networks of type I cells that are close to their excitation thresholds. We analyze the dynamics of two identical Morris-Lecar model neurons coupled by reciprocal inhibition with non-negligible synaptic decay time, and find that an increase in coupling strength destabilizes phase-locking through a period-doubling cascade, leading to the 2:2 frequency-locked alternating-order ("leap-frog") spiking, as well as more complex n:n periodic modes and chaotic dynamics. Similar behavior was recently reported by Maran and Canavier (2007) in *heterogeneous* networks of strongly coupled higher-dimensional type-I excitable cells. We find that leap-frog spiking can be maintained by a completely *homogeneous* two-cell network, and that it arises when the synaptic input is sufficiently strong to transiently bring the postsynaptic cell past the excitation threshold to a fixed equilibrium, pushing the trajectory off the limit cycle. We give an intuitive geometric description of the observed dynamics, and analyze quantitatively these activity states using the first-order spike-time response curve of each cell. Finally, we show that an inter-spike interval return map based on a simple quadratic spike-time response curve can reproduce the entire coupling-strength bifurcation diagram characterizing the dynamics of two coupled type-I oscillators, which illustrates the universality of the described network behavior.

1 Introduction

The question of synchronization of coupled oscillators is of fundamental importance for the understanding of rhythmogenesis in biological networks, and has been a subject of great interest in mathematical biology and neuroscience (Winfree, 2001; Izhikevich, 2006). In order to better understand the dynamics of multi-neuron networks, it is important to fully examine the case of a two-cell network, particularly relevant in the study of central pattern generators which often contain subcircuits composed of pairs of mutually inhibitory cells. When the coupling between oscillators is weak, synchronization and its stability can be analyzed using the well-known geometric phase-reduction approach and the method of averaging (Kuramoto, 1984; Ermentrout and Kopell, 1984, 1990; Hoppensteadt and Izhikevich, 1997; Izhikevich and Kuramoto, 2006). The weak-coupling theory is very general in its applicability, and for a homogeneous two-cell network predicts stable phased-locked firing, either synchronous or anti-synchronous, depending on the properties of the coupling and the intrinsic dynamics of the oscillators (Vreeswijk and Abbott, 1994; Hansel et al., 1995; Ermentrout, 1996). Strongly coupled networks can exhibit a much richer variety of dynamic behaviors, but their analysis presents a much greater challenge, as there is no general method of determining the stable modes of network activity in this case. However, in the case of pulsatile coupling which is lasting only briefly relative to the length of the unperturbed period, the dynamics of strongly coupled networks can be analyzed using Poincaré return maps for the inter-spike intervals, derived from the phase-resetting curves of the coupled cells (Mirollo and Strogatz, 1990; Canavier et al., 1999; Goel and Ermentrout, 2002). The Poincaré firing map approach is also useful in the analysis of strongly coupled relaxation oscillators (Somers and Kopell, 1993; Rubin and Terman, 2000; Izhikevich, 2000). Finally, the return map formalism is very effective in the analysis of integrate-and-fire neuronal networks (Mirollo and Strogatz, 1990; Vreeswijk and Abbott, 1994; Bressloff and Coombes, 2000).

While most of the studies of strongly-coupled networks concentrate on the phase-locked synchrony observed in weakly coupled networks, it is known that strong coupling can destabilize phase-locked dynamics (Ermentrout and Kopell, 1991). For instance, many network models exhibit the transition to the "oscillator death" mode as the coupling strength is increased, whereby some of the neurons become trapped at a fixed point by the strong synaptic currents arriving from the active cell (Ermentrout and Kopell, 1990; Bressloff and Coombes, 1998). Further, several recent studies showed the emergence of more complex non-phase locked states in the case of heterogeneous networks, whereby both neurons are active at different intervals of the oscillation period (Bressloff and Coombes, 2000). In particular, the recent work of Maran and Canavier (2007) revealed that the assumption of preserved firing order does not hold in a heterogeneous network of Wang-Buzsáki model neurons with type-I excitability (Wang and Buzsáki, 1996). They showed the emergence of a 2:2 mode-locked "leap-frog" state (see Fig. 1b), and demonstrated that the second-order phase resetting is important for explaining this behavior in the model they consider.

Here we report that a similar leap-frog alternating-order spiking is a generic property of a *homogeneous* network of two identical type-I Morris-Lecar model neurons coupled by inhibitory synapses with finite synaptic decay time. The network we consider exhibits synchronous firing for weak coupling, which is readily destabilized even by a moderate increase in coupling strength (see Fig. 1b). We show that this is a general property for an inhibitory network of cells which are close to their excitation thresholds. An interesting aspect of the alternating-order spiking is that it cannot be obtained by any phase-reduced model with instantaneous synaptic coupling, but can be described by an extended phase model with an additional passive negative-value phase branch representing the suppressed state of the cell. Further, we show that the first-order phase resetting is sufficient to quantitatively describe this activity state. Finally, we find that the entire coupling-strength bifurcation structure of

the two-cell ML network can be qualitatively reproduced by a simple quadratic STRC. Our results demonstrate that non-phase locked activity is a generic property of inhibitory networks of excitable cells with type-I excitability.

2 Model

We consider a pair of two identical model neurons with type-I excitability (Rinzel and Ermentrout, 1998), each modeled as a Morris-Lecar oscillator (Morris and Lecar 1981). Each cell possesses a periodic limit cycle trajectory corresponding to an action potential, which results from the interplay between the depolarizing calcium current I_{Ca} and the activation w of the repolarizing potassium current, I_K. The two cells are assumed to be identical, and are coupled by an inhibitory synaptic current, $I_{syn}(V,s)$:

$$\begin{aligned} C\frac{dV}{dt} &= -I_{Ca} - I_K - I_L - I_{syn}(V,s) - I_{app} \\ \frac{dw}{dt} &= (w_\infty(V) - w)/\tau_\infty(V) \\ I_{Ca} &= \bar{g}_{Ca} m_\infty(V)(V - V_{Ca}) \\ I_K &= \bar{g}_K w(V)(V - V_K) \\ I_L &= \bar{g}_L(V - V_L) \end{aligned} \tag{1}$$

where the capacitance $C = 1\ \mu F/cm^2$, V is the cell membrane voltage in mV, t is time in ms, I_L is the passive leak current, and $I_{app} = 14\ \mu A/cm^2$ is the applied current.

The steady-state activation of calcium current is

$$m_\infty(V) = \frac{1}{2}(1 + \tanh(\frac{V+12}{18}))$$

The potassium current activation amplitude and activation rate are

$$w_\infty(V) = \frac{1}{2}(1 + \tanh(\frac{V+8}{6}))$$

$$\frac{1}{\tau_\infty(V)} = \frac{2}{3}\cosh[(V+8)/6)]$$

Given this choice of model parameters, each of the two uncoupled oscillators exhibits periodic spiking with a period of about 45 ms. Note that this model is far from the relaxation limit in terms of the time scale separation.

The two cells are coupled through the synaptic current given by

$$I_{syn} = \bar{g}_{syn} s(t)(V - V_{inh})$$

where $\bar{g}_{syn}$ is the maximum synaptic conductance and $V_{inh} = -80\ mV$ is the reversal potential. The dynamics of the synaptic gating variable $s(t)$ depends on the presynaptic cell potential, V_{pre}:

$$\frac{ds}{dt} = \begin{cases} -s/\tau_{syn} & \text{if } V_{pre} < V_{th}, \\ (1-s)/\tau_\gamma & \text{if } V_{pre} > V_{th}. \end{cases} \tag{2}$$

where $V_{th} = -3\ mV$ is the synaptic threshold, and τ_{syn} and $\tau_\gamma = 0.2\ ms$ are the synaptic decay and rising time constants, respectively. We focus primarily on short synaptic decay times of about $\tau_{syn} = 1 - 5$ ms, and discuss separately the observed effect of prolonging τ_{syn}.

Figure 1: Network activity states at different values of coupling strength, $\bar{g}_{syn}$. The potentials of the two cells are shown as red and black traces, respectively. (a) Synchronous phase-locked firing ($\bar{g}_{syn} = 0.03$). The spiking period is close to the unperturbed period of 45 ms. (b) Alternating-order (leap-frog) spiking ($\bar{g}_{syn} = 0.17$) (c) Period-2 alternating-order spiking ($\bar{g}_{syn} = 0.22$) (d) Chaotic state, irregular inter-spike intervals ($\bar{g}_{syn} = 0.29$) (e) Bursting (3:3 alternating-order firing, $\bar{g}_{syn} = 0.34$) (f) Spike-suppress state ("oscillator death", $\bar{g}_{syn} = 0.5$)

Figure 2: Bifurcation diagram of the Morris-Lecar model network. ISI_∞, the asymptotic values of the intervals between consecutive spikes (not necessarily spikes of the same cell) are plotted as a function of the coupling strength, $\bar{g}_{syn}$, for two values of synaptic decay time: (a) $\tau_{syn} = 1$ and (b) $\tau_{syn} = 2$. The dotted lines correspond to each of the six activity states in Figure 1(a)-(f). Note the difference in scale along the $\bar{g}_{syn}$ axis.

3 Results

3.1 Network activity states

We start by exploring in detail the behavior of the system described by Eqs. 1, the two identical ML model neurons with mutually inhibitory synaptic interaction. Figure 1 shows the diversity of behaviors exhibited by this network for different values of the maximal synaptic conductance, $\bar{g}_{syn}$, and the bifurcation diagram presented in Figure 2 demonstrates the transitions between the different activity states. For very small values of this coupling parameter, the two neurons fire in synchrony, as predicted by the weak coupling theory (see below). When $\bar{g}_{syn}$ is increased, the synchronized state loses stability, and the network transitions to the alternating-order 2:2 mode-locked state shown in Figure 1(b), also referred to as "leap-frog" spiking by Maran and Canavier (Maran and Canavier, 2007). In this state, there is a stable non-zero time interval between the spikes of the two cells, with cells changing firing order in each cycle of the oscillation. For yet higher values of the coupling, the interval between the consecutive spikes of the two cells alternates in each cycle between two distinct values, as shown in Figure 1(c). For higher still values of $\bar{g}_{syn}$, the alternating-order firing state undergoes a period-doubling cascade and gives way to the chaotic firing in which the inter-spike intervals and the spiking order change irregularly. Further, for narrow ranges of $\bar{g}_{syn}$ values multi-spike $m : n$ alternating order firing states emerge, as shown in Figure 1(e), which represent a form of bursting. Finally, very strong coupling leads to the so-called "oscillator death" state shown in Figure 1(f), whereby the spiking of one neuron provides enough inhibition to completely prevent the spiking of the partner cell (Ermentrout and Kopell, 1990; Bressloff and Coombes, 1998).

Bifurcation diagram presented in Figure 2 explores the transitions between these different behaviors, showing the coupling-strength dependence of the asymptotic (equilibrium) intervals between two consecutive network spikes, which may or may not be the spikes of the same cell. These inter-spike intervals are normalized to the period of the uncoupled cell, and are denoted ISI_∞. The values of $\bar{g}_{syn}$ corresponding to each of the activity states shown in Figure 1 are marked by vertical dashed lines. Even though the set of ISI_∞ values does not fully characterize the network state, since it does not explicitly contain information about the spiking order of the two cells, it allows one to easily infer the dynamics at any given value of $\bar{g}_{syn}$. Note in particular that the presence of the value $ISI_\infty \approx 1$ indicates that at least one of the cell spikes twice in a row in each cycle, without the interference from the other cell. This is only possible if the cells change their firing order in each oscillation cycle. The fact that the interval between the spikes of the same cell in Figure 1(b)-(c) is close to the unperturbed period indicates that the second-order phase resetting is not crucial for the alternating order state, and that the first-order phase resetting dominates (cf. Maran and Canavier, 2007). It is one of our main goals to provide a simple geometric explanation and quantitative analysis of the alternating-order

Figure 3: Effect of an increase in coupling strength on the stability of phase-locked firing in an excitatory network (a) and an inhibitory network (b). $\bar{g}_{syn}$ changes from 0.01 to 0.2 in both cases. In the case of excitation (a), anti-phase synchronous firing is stable for a wide range of coupling strength, while the phase-locked synchronous firing is readily destabilized in the case of mutual inhibition (b).

spiking behavior seen in Figure 1(b)-(c), and to explain the period-doubling cascade evident in Figure 2.

Figure 2(b) presents the bifurcation diagram for a larger value of the synaptic decay time constant ($\tau_{syn} = 2$ as opposed to $\tau_{syn} = 1$ used in all the simulations in this paper), and demonstrates that the qualitative features of the network behavior are the same for a range of τ_{syn} values. The main effect of prolonging synaptic decay is to increase the total amount of inhibition that each cell receives from its partner, thereby compressing the bifurcation diagram along the $\bar{g}_{syn}$ axis. The dynamics of the network undergoes a significant change only for values of τ_{syn} beyond about 6 ms, or roughly 1/8 of the unperturbed period of 45 ms. For these longer values of synaptic decay time, the second order STRC becomes non-negligible, and the alternating-order state can only be achieved for a narrower range of the synaptic conductance parameter (see Discussion).

3.2 Destabilization of phase-locked firing: comparison of excitation and inhibition

In the case of two type-I excitable cells with continuous synaptic interaction, the weak coupling theory predicts stable anti-synchronous and synchronous firing for excitatory and inhibitory synaptic coupling, respectively (Vreeswijk and Abbott, 1994; Hansel et al., 1995; Ermentrout, 1996). As demonstrated in Figure 3, this agrees with the dynamics exhibited by our model in the case of small synaptic conductance (top panels, $\bar{g}_{syn} = 0.01$). As the synaptic conductance is increased however, there is a qualitative difference between the stability of phase-locked firing in the case of excitation versus inhibition. Namely, the anti-synchronous state remains stable for strong excitatory coupling (see Figure 3(a)), but an increase in inhibitory coupling quickly destabilizes phase-locking and leads to the alternating-order state shown in Figure 3(b).

This difference between the effects of non-weak excitation and inhibition becomes obvious when one considers the phase plane dynamics of the system. Figure 4 illustrates schematically the effect of non-weak synaptic interaction on the phase-plane dynamics of the post-synaptic cell. Note that there is no qualitative change in the geometry for a wide range of excitatory conductances. However, an obvious qualitative change occurs when the inhibition strength becomes sufficiently strong to suppress the cell below its excitation through the saddle-node on the invariant cycle bifurcation (Hoppensteadt and Izhikevich, 1997). If such suppression last for the entire period of the oscillation, the oscillator death occurs ("spike-suppress" state, Fig. 1(f)). However, for intermediate strength of inhibitory coupling, the suppression occurs only for part of the oscillation period, resulting in a transient sub-threshold trapping of each cell during each cycle of the oscillation. This leads to the alternation of the firing order (Fig. 1(b),(c)), whereby one cell is able to bypass its partner cell along the limit cycle by transiently keeping the other cell in the passive branch of the trajectory, as depicted in Fig. 5. Therefore, synchrony in networks of type-I oscillators should be readily destabilized even for moderate increase in inhibitory coupling. This result is quite general and is not specific to the Morris-Lecar model cells that we consider. In particular, it is probable that the same mechanism is at play in the case of Wang-Buzsáki oscillators (Wang and Buzsáki, 1996) studied by Maran and Canavier (2007).

Figure 4: Effect of non-weak coupling on the phase-plane trajectory of the postsynaptic cell. Double arrows indicate the movement of the V-nullcline during each cycle of the network oscillation. (a) In the case of excitation, an increase in synaptic coupling causes no qualitative change in the phase plane geometry. (b) For sufficiently strong inhibition, the V-nullcline of the post-synaptic cell intersects the w-nullcline with each presynaptic input, pushing the cell below the excitation threshold and off the limit cycle trajectory. Thick blue curve indicates the trajectory of each cell during one cycle of the alternating-order spiking shown in Fig. 1(b),(c)

Figure 5: Phase plane dynamics of the two coupled cells during periodic leap-frog alternating-order spiking (top left trace). The tadpole-shaped curves schematically represents the phase plane trajectory in Figure 4(b). The sequence of five panels describe the phase-plane dynamics underlying the spike sequence shown in top left panel: (i) "red" cell spikes; (ii) "blue" cell spikes, lowering the nullcline of the red cell, and trapping it in the passive phase of the trajectory (tadpole tail); (iii) termination of the blue cell's spike; red cell gradually recovers from inhibition; (iv) blue cell bypasses the red cell 1 along the unperturbed limit cycle trajectory; (v) blue cell spikes again, followed by the spike of the red cell. The process then repeats itself, with red cell emitting the next spike.

3.3 Phase-reduced descriptions

It is instructive to examine the observed non-synchronous dynamics in the context of the weak-coupling theory (reviewed in Hoppensteadt and Izhikevich, 1997; Rinzel and Ermentrout, 1998; Izhikevich and Kuramoto, 2006). The standard weak coupling synchronization analysis relies on the following three crucial assumptions: (i) unique exponentially attracting limit cycle (hyperbolicity condition), whose neighborhood is foliated by unique isochrons, allowing phase description of the trajectory; (ii) coupling is weak, allowing linearization of the isochrons; (iii) perturbation of phase due to the coupling is much smaller than the unperturbed period, allowing averaging. These assumptions enable one to describe the dynamics of the coupled network using phase deviation model:

$$\begin{aligned} \dot{\phi}_1 &= 1 + H_{12}(\phi_1, \phi_2) \\ \dot{\phi}_2 &= 1 + H_{21}(\phi_2, \phi_1) \end{aligned} \tag{3}$$

where $\phi_i \in [0, 1]$ is a phase deviation ($i, j = 1, 2$), and $H_{ij}(\cdot)$ is the connection function.

We now show that neither our model nor any other model possessing an alternating-order firing state can be approximated by such a 2D coupled-phase description.

The Figure 6(a) schematically illustrates the general topology of the 2:2 periodic alternating-order firing state in terms of the corresponding (ϕ_1, ϕ_2) phase plane trajectory (not necessarily describing our ML network). Here the right and top boundary values ($\phi_{1,2} = 1$) correspond to the peak of an

Figure 6: Reduced phase description of the alternating-order state. (a) In the model with continuous synaptic interaction, the alternating-order spiking is a continuous trajectory on the 2-torus. The spike times of the two cells correspond to the intersections of the trajectory with the $\phi_1 = 1$ and the $\phi_2 = 1$ boundaries, respectively. The change in spiking order requires the trajectory to self-intersect. The dashed gray lines indicate the formal equivalence of the continuous coupling description to the pulse-coupled model description shown in (b). In (b), the spike of cell i ($\phi_i = 1$) causes a discontinuous drop (red arrow) in the phase of the partner cell j by amount $\Delta(\phi_j)$, where $\Delta(\phi)$ is the spike-time response characteristic of the cell (which we define to be positive in case of a phase delay). The change in firing order requires the phase domain to be extended to the passive negative value branch. In order for the spiking order to change, the value of the spike-time response $\Delta(\phi)$ should be greater than ϕ for one of the two spikes that each cell emits in one cycle of the oscillation.

action potential of the respective cell. In the case of continuous synaptic interaction (as in our model), the periodic trajectory is a continuous closed curve on the (ϕ_1, ϕ_2) torus, and its curvature is a measure of synaptic current that deflects the trajectory from a straight line. Note that the trajectory must self-intersect in order for the cell spike order to change in each cycle of the oscillation. Therefore, the network exhibiting alternating-order firing cannot be described in terms of the phase system given by Eqs. 3. In particular, it is clear that the averaging transformation that defines the coupling functions H_{ij} in Eqs. 3 cannot be carried out in our case since the phase perturbation in each cycle is not an infinitesimal quantity relative to the oscillation period.

However, the phase topology of Figure 6(a) provides an entirely valid description of a 2:2 activity state if it is viewed as a projection of a higher-dimensional trajectory onto the (ϕ_1, ϕ_2) plane. The additional degrees of freedom in our model are the two synaptic gating variables $s_{1,2}(t)$ that evolve according to Eqs. 2. Thus, we conclude that the leap-frog spiking implies the presence of hidden "memory" variables in the system, which in this case are the synaptic gating variables. A corollary of this fact is that the finite synaptic decay time course is indispensable in order for a network to exhibit the change in firing order in the steady state.

Figure 6(b) shows an alternative phase topology of the 2:2 leap-frog state, which formally can be viewed as the limit of the Figure 6(a) with respect to shortening the duration of the synaptic current ("straightening out" the trajectory), while keeping fixed the total amount of phase resetting. Here the synaptic interaction is no longer continuous, but purely pulsatile (delta-function coupling). Although the two descriptions are formally equivalent in terms of their spike-time phase-resetting values, this second description is qualitatively different in that it requires the extension of the phase domain to negative values, and therefore is not a true phase-reduced description. The negative phase value is induced when the phase resetting is greater than the inter-spike phase difference between the two cells, i.e. $\Delta(\phi) > \phi$, where $\Delta(\phi)$ is the spike-time response curve, STRC (note that we define $\Delta(\phi)$ to be positive if the synaptic input produces a phase delay). Thus, the alternating-order firing state can also be obtained in the framework of a phase model with instantaneous coupling, if the phase domain is supplanted with a negative value branch. In particular, the 2:2 mode in question is a possible activity state in an appropriately modified model network of pulse-coupled one-dimensional integrate-and-fire neurons, known for their tadpole-like phase structure.

In the ML model network we consider, the synaptic decay time is short relative to the unperturbed limit cycle period, and therefore the dynamics of our model is closer to the phase diagram of Figure 6(b) rather than Figure 6(a). In our case the negative phase represents the suppression of a cell into the passive "tadpole" branch of the periodic trajectory during the peak of inhibition (Figures 4(b), 5), allowing the other cell to pass ahead, reversing the order of two cells. However, as we noted above, the finite synaptic decay time is essential, since it allows the temporary suppression of each cell by its partner, creating the passive negative phase branch.

3.4 Analysis of existence and stability of periodic alternating-order firing

Although Figures 5-6 explain qualitatively the dynamics of the alternating-order firing state, we turn to the phase return map approach to study it on a quantitative level, and to analyze its stability. The return map analysis is a powerful method of describing the dynamics of a coupled network, and requires less assumptions than the weak-coupling reduction given by Eqs. 3. Importantly, it requires that the cell's spike width and amplitude are invariant and are not affected by the coupling incoming from the other cell. One also assumes that the perturbation only affects the time to the next spike of the perturbed cell, and has no effect on the dynamics of the cell thereafter. However, this method

Figure 7: Constructing the inter-spike phase return map for the periodic alternating-order spiking, $\phi_1 \to \phi_2 = \Phi(\phi_1)$. (a) In each cycle of the alternating-order spiking, one of the cells spikes twice (dashed red lines at times t_1 and t_2) between two spikes of the partner cell (black lines). The phase variables ϕ_1 and ϕ_2 are inter-spike intervals normalized by the unperturbed period of each oscillator. Note that the phase difference between two red spikes equals 1 (the unperturbed period). The phase of the cell at the time of arrival of the second input is $1 + \phi_1 - \Delta(\phi_1)$, where $\Delta(\phi_1)$ is the phase delay due to the arrival of the first input. (b) Black curve represents the STRC of each ML oscillator, $\Delta(\phi)$, while the blue curve represents the return map $\Phi(\phi)$ (Eqs. 12). The synaptic coupling strength is $\bar{g}_{syn} = 0.09$

is easily extended to the case where perturbation affects several periods of the post-synaptic cell. In fact, Maran and Canavier (2007) demonstrated the emergence of the alternating-order firing in a heterogeneous network of inhibitory coupled type I model cells in the presence of significant second order phase resetting. Here we demonstrate that the alternating-order firing emerges even in our homogeneous network with only 1st order phase-response effects.

The alternating-order firing is completely characterized by the inter-spike phase sequence labeled $\{\phi_1, \phi_2\}$ in Figure 7(a). Here we will construct the return map relating these phase differences, using the phase-resetting curve, or the spike-time response curve (STRC) of each cell, $\Delta(\phi)$. We define $\Delta(\phi_1)$ to be positive if it produces a phase delay, and negative if it produces a phase advance. The derivation below is a simplified version of a more general return map derived by Maran and Canavier (2007) for the case of second-order phase resetting.

Suppose that t_1 denotes the arrival time of the first synaptic current pulse due to the spike of the pre-synaptic cell (red spike in Fig. 7(a)). $\Delta(\phi_1)$ determines the amount of phase delay induced at time t_1, where $\phi_1 = t_1/T_o$ is time normalized by the unperturbed period of each oscillator, T_o (See Fig. 7(a)). The inhibition due to sufficiently strong phase resetting satisfies $\Delta(\phi) > \phi$, which delays the time to next spike of the post-synaptic cell to a value beyond the intrinsic (uncoupled) oscillation period T_o. As a result, the pre-synaptic cell has a chance to spike again (red spike in Fig. 7(a)) after time interval T_o, corresponding to the unperturbed phase period of $\phi = 1$. This second synaptic current from same pre-synaptic cell arrives at time t_2, at which point the phase of the post-synaptic cell equals $\xi_1 \equiv 1 + \phi_1 - \Delta(\phi_1)$, which takes into account the delay due to the first spike. Therefore, the second spike induces a phase delay equal to $\Delta(1 + \phi_1 - \Delta(\phi_1))$. It is only after receiving this second pre-synaptic input that the post-synaptic cell has finally a chance to spike, after a phase delay of ϕ_2 following the second input. The total phase delay due to both inputs is thus equal to

$$\frac{T' - T_o}{T_o} = \phi_1 + \phi_2 = \Delta(\phi_1) + \Delta(1 + \phi_1 - \Delta(\phi_1))$$

where T' is the new interval between consecutive spikes of the one cell enclosing two spikes of the partner cell. Then the return map for the phase intervals ϕ_i is given by

$$\phi_2 \equiv \Phi(\phi_1) = \Delta(\phi_1) + \Delta(1 + \phi_1 - \Delta(\phi_1)) - \phi_1$$

or, expressed in terms of the phase of the post-synaptic cell at the time of arrival of the second spike, $\xi_1 = 1 + \phi_1 - \Delta(\phi_1)$:

$$\phi_2 \equiv \Phi(\phi_1) = 1 + \Delta(\xi_1) - \xi_1 \tag{4}$$

Fixed points of this map correspond to the periodic 2:2 alternating-order (leap-frog) activity:

$$\phi = 1 + \Delta(\xi) - \xi \tag{5}$$

Figure 8: Phase-map analysis of the alternating-order spiking. (a) The cell potential time courses of the two coupled ML oscillators are shown in red and black, respectively, for $\bar{g}_{syn} = 0.2$. (b) Equilibrium inter-spike phase difference ($\phi = 0.144$) in the alternating-order state satisfies Eq. 5, which can be re-written as $\Delta(1-\psi) = \phi - \psi$ in terms of the quantity $\psi = 1 - \xi = \Delta(\phi) - \phi$. In this simulation, $\psi = \Delta(\phi) - \phi = 0.0468$, and $\Delta(1-\psi) = 0.095$. The stability condition is given by Eq. 9: $|[1-\Delta'(1-\psi)][\Delta'(\phi)-1]| < 1$. (c) Inter-spike phase sequence artificially generated (emulated) by the phase return map $\Phi(\phi)$ (Eqs. 4) using the simplified quadratic STRC shown in (d). (d) Quadratic spike-time response curve $\Delta(\phi) = 4m\phi(1-\phi)$, where $m = 0.5$ is the maximum phase resetting.

Since $\xi \equiv 1 + \phi - \Delta(\phi)$, this condition can be written in a more symmetric form

$$\phi = \frac{\Delta(\phi) + \Delta(\xi)}{2} \tag{6}$$

Taking into account the constraint on the phase domains, $\xi \leq 1$ and $\Phi(\phi) \leq 1$, we also obtain

$$\Delta(\phi) \geq \phi \tag{7}$$

$$\Delta(\xi) \leq \xi \tag{8}$$

Conditions 6-8 are examined geometrically in Figure 8. Note that the synchronous firing solution $\{\phi = 0^+, \xi = 1^-\}$ always satisfies these periodicity conditions, if one assumes $\Delta(0^+) = \Delta(1^-) = 0$.

If the inequality $\xi \leq 1$ is violated (i.e. when $\Delta(\phi) < \phi$), the cells fire sequentially, so their firing order does not alternate, while the violation of the condition $\Phi(\phi) \leq 1$ (i.e. if $\Delta(\xi) > \xi$) indicates that the postsynaptic cell will emit more than two consecutive spikes. The latter is true for instance for n:n bursting states with $n > 2$ (see Fig. 1(d)), in which case one can derive an extended map analogous to Eq. 4. An additional alternating-order constraint $\Phi(\phi) \geq 0$ requires that $\Delta(\xi) > -(1-\xi)$. This condition is automatically satisfied if the resetting is sign-definite (pure delay resetting).

Stability of the 2:2 periodic spiking depends on the value of the derivative of the phase map given by Eq. 4 at equilibrium:

$$\Phi'(\phi) = [1 - \Delta'(\xi)][\Delta'(\phi) - 1] \tag{9}$$

The fixed point will be stable if $|\Phi'(\phi)| < 1$. Therefore, the periodic alternating-order firing is stable when the slope of the STRC at the time of arrival of either of the two synaptic inputs (corresponding to phases ϕ and $\xi = 1 + \phi - \Delta(\phi)$) is sufficiently close to 1. This is equivalent to the stability condition derived by Maran and Canavier (2007). The stability of synchronous firing is determined by the same map slope expression, with $\phi = 0^+$ and $\xi = 1^-$ (Goel and Ermentrout, 2002). Since $\Delta'(1) \approx 0$ in the Morris-Lecar model (see Fig. 9), the bifurcation from synchronous to leap-frog firing occurs when the slope $\Delta'(\phi)$ at $\phi = 0$ becomes greater than 2, forcing ϕ to increase (and thus ξ to decrease) until the stability condition is satisfied. Thus, the characteristic sharp initial rise of $\Delta(\phi)$ followed by a less steep increase at larger ϕ, seen both in Fig. 9 of this work, and in Fig. 2(b) of Maran and Canavier (2007), is essential for the transition from synchronous to leap-frog spiking.

We find that the initial STRC slope $\Delta'(0)$ is smaller for larger values of synaptic decay time. This explains the bistability between alternating-order and synchronous spiking that we observe at larger τ_{syn} (see Discussion).

3.5 Second-order STRC

Figure 9 shows that the second-order phase resetting ($\Delta_2(\phi)$) is non-zero only for phase values close to 1, since the synaptic time constant is short ($\tau_{syn} = 1-2$ ms). For the two characteristic phases

Figure 9: Comparison between the first- and the second-order spike-time response curves of the Morris-Lecar oscillator. The first-order STRC is shown in blue, while the second-order STRC is shown in red, for synaptic conductance of $\bar{g}_{syn} = 0.2$. The two functions satisfy the consistency (periodic boundary) condition $\Delta(0) = \Delta_2(1)$, where $\Delta(\phi)$ and $\Delta_2(\phi)$ are the first- and the second-order STRC, respectively. The second-order phase resetting provides only negligible contribution to the alternating-order firing (cf. Fig. 8(a)): $\Delta_2(\phi) = 0$; $\Delta_2(\xi) = 1.4 \cdot 10^{-4}$.

in Fig. 8(a), the second-order phase resetting values equal $\Delta_2(0.144) \approx 0$ and $\Delta_2(0.9592) \approx 1.4 \cdot 10^{-4}$. Therefore, second-order resetting provides only negligible contribution to the alternating-order periodic firing shown in Fig. 8(a). This is to be contrasted with the behavior of a heterogeneous network studied by Maran and Canavier (2007), who showed that leap-frog spiking could not be achieved without 2-nd order phase resetting in the parameter regime that they considered. This may be a result of more significant second-order phase resetting in their model (see Fig. 2(b) *ibid.*).

Although we find that the second-order phase resetting is not critical to achieving stable alternating-order activity, it will influence the critical value of $\bar{g}_{syn}$ at the bifurcation from synchrony to leap-frog spiking, since it affects the stability of both states. Noting once again that the second-order phase-resetting is negligible for small values of the phase, we find that the map slope previously given by Eq. 9 is modified according to (see Appendix for derivation):

$$\Phi'(\phi) \quad = \quad [1 - \Delta'(\xi)][\Delta'(\phi) - 1] + \Delta_2'(\xi) \tag{10}$$

In particular, synchronous firing is stable if

$$|[1 - \Delta'(1)][\Delta'(0) - 1] + \Delta_2'(1)| < 1 \tag{11}$$

Further, taking into account the small slope of the first-order STRC at $\phi = 1$ (see Fig. 9), we obtain an approximate condition

$$|\Delta'(0) + \Delta_2'(1) - 1| < 1$$

Since both derivatives are positive, synchrony is stable if

$$\Delta'(0) + \Delta_2'(1) < 2$$

Therefore, the bifurcation between synchronous and leap-frog spiking occurs when $\Delta'(0) + \Delta_2'(1) = 2$. The stability condition (Eq. 10) suggests that second-order phase resetting has a generally destabilizing effect on both synchronous and alternating-order activity. This agrees with our finding that stable alternating-order spiking cannot be achieved when τ_{syn} is comparable to the length of the uncoupled oscillation period.

3.6 Simplified STRC

Given the knowledge of the STRC, one can readily determine the stable network activity modes for the corresponding value of the coupling strength. However, the full range of activity states demonstrated in the bifurcation diagram of Figure 2 requires one to know the STRC at each value of the synaptic conductance. In the case of weak coupling, the STRC is assumed to scale linearly with the strength of the coupling, a condition which is violated in the case of non-weak interactions that we consider. In particular, the right-ward shift in the peak of the STRC curve evident in Figure 7(b) is a well-known feature of the Morris-Lecar model (Ermentrout, 1996). The question then arises about

Figure 10: Period-2 (unequal phase) alternating-order leap-frog spiking emulated using the quadratic STRC (a) Inter-spike phase sequence generated by the emulator is similar to the period-2 leap-frog spiking exhibited by the ML network, shown in Figure 1(c). The stable phase differences are $\phi_1 = 0.254$ and $\phi_2 = 0.463$. (b) The period-2 leap-frog existence conditions (Eqs. 13) are satisfied for the quadratic STRC $\Delta(\phi) = 4m\phi(1-\phi)$, where $m = 0.55$ is the peak phase resetting.

Figure 11: Emulated bifurcation diagram for the inter-spike interval differences as a function of synaptic conductance for the quadratic STRC. Asymptotic inter-spike interval differences ISI_∞ are plotted as a function of the STRC peak amplitude, m.

the generality of the bifurcation structure of the network dynamics shown in Figure 2. In particular, we want to find out whether this observed state transition sequence is specific to the ML model we consider.

In order to address the question, we replace the numerically generated STRC with a simple quadratic relationship, $\Delta(\phi) = m\phi(1-\phi)$. Then, we employ the "emulator" algorithm introduced by Canavier et al. (1999), i.e. we use the STRC to artificially generate the "inter-spike" phase sequence, as shown in Figure 10. We explore the effect of increasing coupling strength by increasing the STRC amplitude, m, the linear scaling factor of the quadratic.

Figures 8(d) and 10(b) show that both the period-1 and the period-2 alternating order spiking conditions can be achieved using the quadratic STRC (see below for the description of the period-2 state). Although the analytic equilibrium solutions of the return map cannot be obtained in either case, the equilibrium phases are readily obtained numerically, and are labeled in Figures 8(c) and 10(a). More importantly, the entire bifurcation structure of the ML network dynamics is reproduced by the quadratic STRC emulator, as shown in Figure 11.

Note that the map amplitude corresponding to the bifurcation from synchronous to alternating-order firing can be obtain analytically for the case of quadratic PRC using Eq. 9: $\Phi'(0) > 1$ for $m > m_{crit} = 2^{-3/2} \approx 0.35355$ (cf. Fig. 10). The bifurcation to the oscillator death is also easily analyzed, and occurs at $m = 1$.

3.7 Existence and stability of period-2 alternating-order spiking

If the intervals ϕ_1 and ϕ_2 between the spikes of the pre- and the post-synaptic cell alternate between two distinct values, as in Figure 1(c), we call the corresponding periodic state period-2 alternating-order 2:2 firing, since it results from the period-doubling of the equal-phase alternating-order state (Fig. 2).

Both ϕ_1 and ϕ_2 are period-2 fixed points of map given by Eq. 5, i.e. $\Phi(\Phi(\phi_{1,2})) = \Phi(\phi_{2,1}) = \phi_{1,2}$, therefore

$$\begin{aligned} \Phi(\phi_1) &= 1 + \Delta(\xi_1) - \xi_1 = \phi_2 \\ \Phi(\phi_2) &= 1 + \Delta(\xi_2) - \xi_2 = \phi_1 \end{aligned} \tag{12}$$

where $\xi_i = 1 + \phi_i - \Delta(\phi_i)$, $i = 1, 2$. To analyze whether a given STRC is consistent with these conditions, which we do in Fig. 10(b), it is convenient to re-write the existence conditions given by Eq. 12 in terms of the quantities $\psi_i = 1 - \xi_i = \Delta(\phi_i) - \phi_i$:

$$\begin{aligned} \Phi(\phi_1) &= \Delta(1 - \psi_1) + \psi_1 = \phi_2 \\ \Phi(\phi_2) &= \Delta(1 - \psi_2) + \psi_2 = \phi_1 \end{aligned} \tag{13}$$

Figure 12: The network of three all-to-all coupled ML oscillators can exhibit splay states in a certain range of synaptic coupling strength ($\bar{g}_{syn} = 0.14$). The potentials of the three cells are shown as black, red, and blue traces. Note the change in spiking order: 1,2,3 → 3,2,1 → 1,2,3 → ...

Stability is given by the derivative of the map $F(\phi) = \Phi(\Phi(\phi))$ at equilibrium values ϕ_1 and ϕ_2:

$$\begin{aligned} F'(\phi_{1,2}) &= \Phi'(\phi_2)\Phi'(\phi_1) \\ &= [1 - \Delta'(\xi_1)][\Delta'(\phi_1) - 1][1 - \Delta'(\xi_2)][\Delta'(\phi_2) - 1] \end{aligned}$$

The fixed point will be stable if $|F'(\phi_{1,2})| = |\Phi'(\phi_2)\Phi'(\phi_1)| < 1$, which holds if the slope of the STRC is sufficiently close to one at any of the four equilibrium phases defining the period-2 alternating order state, labeled in Figure 10.

3.8 Network of three or more cells

In order to explore the effects of non-weak inhibitory coupling in a larger network, we simulated the dynamics of three identical neuron with all-to-all coupling, and observed a diversity of network behaviors that are analogous to the activity states exhibited by a two-cell network. As the coupling strength ($\bar{g}_{syn}$) is increased, the synchronized state becomes unstable, giving way to the alternating order state shown in Figure 12, which is followed by a period-doubling cascade to chaotic activity, and at sufficiently strong value of the coupling we observe the transition to the oscillator death mode. Note that in the three-neuron network, the alternating order state represents a splay state (Fig. 12). Our results are in agreement with the results of Maran and Canavier (2007) for the heterogeneous network of Wang-Buzsáki model neurons.

Kuramoto showed that in an all-to-all weakly coupled network, an increase in the coupling strength can overcome heterogeneity in intrinsic cell frequencies, and causes a phase transition from an asynchronous firing to a partially synchronized state (Kuramoto, 1984). An opposite effect is likely to occur in the homogeneous all-to-all network of non-weakly coupled inhibitory cells: while the firing remains synchronous for weak coupling strength, at sufficiently strong value of the coupling the network activity becomes non-synchronous.

4 Discussion

We have shown that phase-locked firing of coupled type-I oscillators becomes destabilized if the inhibition from one cell is sufficient to transiently bring the post-synaptic cell below the excitation threshold. In this case, the two cell network will exhibit leap-frog (alternating-order) spiking, which was also demonstrated recently by Maran and Canavier (2007) in the case of a heterogeneous network of type-I oscillators. Thus, the range of applicability of the weak coupling results may be quite narrow in inhibitory networks of type I oscillators that are close to their excitation thresholds (Hoppensteadt and Izhikevich, 1997). As the coupling strength is increased, the leap-frog spiking state gives way to a period-doubling cascade, leading to more complex m:n bursting states, as well as chaotic activity. Finally, at sufficiently strong values of the coupling strength oscillator death occurs, whereby only one of the cells continues spiking, suppressing the activity of the post-synaptic cell.

Here we proved that the leap-frog dynamics cannot be achieved by a standard phase reduction of the coupled system, and that more than two degrees of freedom are required to obtain leap-frog spiking

in a model with continuous coupling function. However, we also demonstrated that the alternating-order spiking in the network of two ML model neurons can be described entirely in terms of the augmented phase model with the phase domain extended to negative values, which represents the suppression of each cell below the excitation threshold in each cycle of the oscillation. In fact, the entire bifurcation structure of the network activity as a function of the synaptic coupling can be explained by the first-order spike-time response curve. Finally, we show that the network dynamics we report is not specific to the details of the model and the coupling, since the same activity states and the transitions between them can be obtained in an emulated network of phase oscillators with a simplified quadratic phase-resetting curve. We note that the topology of the augmented phase model is similar to the topology of an integrate-and-fire model. Therefore, it should be possible to achieve alternating-order spiking in a network of appropriately modified integrate-and-fire model neurons.

Our results hold in a certain range of synaptic decay times that are significantly shorter than the uncoupled period of each cell. We observe that the second-order phase resetting effects become significant and can no longer be ignored when the synaptic decay time becomes larger than about 1/8 of the unperturbed oscillation period. In this case we see significant bistability between the synchronous and alternating-order states, which is consistent with the stability analysis results that we presented. As the synaptic decay time is increased, the region of attraction of the leap-frog state shrinks. For sufficiently large τ_{syn}, the homogeneous network is no longer capable of sustaining leap-frog activity, and significant heterogeneity may be required to destabilize phase-locking; this conjecture is in agreement with the results of Maran and Canavier (2007), who have observed leap-frog spiking only in a heterogeneous network of type-I oscillators.

Alternating-order firing has was also found previously in homogeneous networks of two coupled relaxation oscillators with excitatory synapses by Bose et al. (2000) and with inhibitory synapses by Sato and Shiino (2007). However, in both works the stable phase difference between the successive spikes of the two cells is much smaller than the width of an action potential. This is also true for the activity states studied by Maran and Canavier (2007). For this reason, earlier studies referred to the alternating-order spiking as a nearly-synchronous state. In contrast, we have shown that the interval between the neighboring spikes of the two cells can constitute more than one half of the resting oscillation period. This is particularly true for the period-2 leap-frog spiking, in which case the interval between the spikes of the two cells can reach 70% of the unperturbed period, and is order of magnitude longer than the decay time of synaptic inhibition (see Fig. 2(a), $\bar{g}_{syn} = 0.23$.). Thus, the alternating-order spiking that we consider represents a distinct activity state that cannot be described as a nearly synchronous state.

Our results and the results of Maran and Canavier (2007) show that even the most simple inhibitory networks of cells with type-I excitability may in general produce a periodic output with complex temporal structure, which may have implications for the understanding of the dynamics of central pattern generators that often contain subnetworks of several cells coupled by reciprocal inhibition. It would be interesting to explore whether the phenomenon we describe is even more general, and whether similar dynamical behavior is exhibited by non-weakly coupled networks of type-II cells, for instance Hodgkin-Huxley model neurons. Note that the crucial condition for the existence of the alternating-order state is the condition on the size of phase-resetting for small values of the phase, $\Delta(\phi) > \phi$. Since the phase-resetting of type-II cells often has an opposite sign for small phase values, we conjecture that the spiking order alternation may be possible in *excitatory* networks of type-II neurons. Further study is required to verify this suggestion.

ACKNOWLEDGMENTS

This work was supported by the National Science Foundation grant DMS-0417416. We wish to thank Amit Bose and Farzan Nadim for helpful comments and discussions.

References

[1] Bose A, Kopell N and Terman D (2000) *Almost synchronous solutions for pairs of neurons coupled by excitation.* Physica D 140:69-94.

[2] Bressloff PC and Coombes S (2000) *Dynamics of strongly-coupled spiking neurons.* Neural Computation 12:91-129.

[3] Bressloff PC and Coombes S (1998) *Desynchronization, mode locking, and bursting in strongly coupled integrate-and-fire oscillators.* Phys. Rev. Lett. 81:2168-2171.

[4] Canavier CC, Baxter DA, Clark JW and Byrne JH (1999) *Control of multistability in ring circuits of oscillators.* Biol. Cybernetics 80:87-102.

[5] Coombes S and Lord GJ (1997) *Desynchronization of pulse-coupled integrate-and-fire neurons.* Phys. Rev. E. 55:2104-2107

[6] Coombes S and Lord GJ (1997) *Intrinsic modulation of pulse-coupled integrate-and-fire neurons.* Phys. Rev. E. 56:5809-5818

[7] Dror RO, Canavier CC, Butera RJ, Clark JW and Byrne JH (1999) *A mathematical critereon based on the phase response curves for stability in a ring of coupled oscillators.* Biol. Cybern. 80:11-23.

[8] Ermentrout GB (1996) *Type I membranes, phase resetting curves, and synchrony.* Neural Computation 8:979-1001.

[9] Ermentrout GB and Kopell N (1984) *Frequency plateaus in a chain of weakly coupled oscillators.* SIAM J. Math. Anal. 15: 215-237.

[10] Ermentrout GB and Kopell N (1990) *Oscillator death in systems of coupled neural oscillators.* SIAM J. Applied Math. 50:125-146.

[11] Ermentrout GB and Kopell N (1991) *Multiple pulse interactions and averaging in systems of coupled neural oscillators.* J. Math. Biol. 29:195-217.

[12] Goel P and Ermentrout GB (2002) *Synchrony, stability, and firing patterns in pulse-coupled oscillators.* Physica D. 163:191-216

[13] Hansel D, Mato G and Meunier C (1995) *Synchrony in excitatory neural networks.* Neural computation 7:307-337.

[14] Hoppensteadt and Izhikevich (1997) *Weakly connected neural networks.* New York: Springer-Verlag.

[15] Izhikevich EM (1999) *Weakly pulse-coupled oscillators, FM interactions, synchronization, and oscillatory associative memory.* IEEE Transactions on neural networks. Vol.10 No.3:508-526

[16] Izhikevich EM (2000) *Phase Equations For Relaxation Oscillators.* SIAM J. Applied Math., 60:1789-1805.

[17] Izhikevich EM (2006) *Dynamics systems in neuroscience: The geometry of excitability and bursting.* Chapter 10: Synchronization. Cambridge, Massachusetts: MIT Press.

[18] Izhikevich EM and Kuramoto Y (2006) *Weakly Coupled Oscillators.* Encyclopedia of Mathematical Physics, Elsevier, 5:448.

[19] Kuramoto Y (1984) *Chemical Oscillations, Waves, and Turbulence.* Springer, Berlin.

[20] Maran SK and Canavier CC (2007) *Using phase resetting to predict 1:1 and 2:2 locking in two neuron networks in which firing order is not always preserved.* J. of Comput. Nerosci., DOI:10.1007/s10827-007-0040-z.

[21] Mirollo RE and Strogatz SH (1990) *Synchronization of pulse-coupled biological oscillators.* SIAM J. APPL. MATH 50:1645-1662.

[22] Morris C, Lecar H (1981) *Voltage oscillations in the barnacle giant muscle fiber.* Biophys J 35: 193–213.

[23] Oprisan SA and Canavier CC (2002) *The influence of limit cycle topology on the phase resetting curve.* Neural Computation 14:1027-1057.

[24] Rinzel J and Ermentrout B (1998) *Analysis of Neural Excitability and Oscillations.* In: Methods in Neuronal Modeling From Ions to Networks, Eds. Koch C and Segev I. MIT Press, Cambridge, MA.

[25] Rubin J and Terman D (2000) *Geometric analysis of population rhythms in synaptically coupled neuronal networks.* Neural Computation 12:597-645.

[26] Sato YD and Shiino M (2007) *Generalization of coupled spiking models and effects of the width of an action potential on synchronization phenomena.* Phys. Rev. E 75:011909:

[27] Somers D and Kopell N (1993) *Rapid synchronization through fast threshold modulation.* Biol Cybern. 68:393-407.

[28] van Vreeswijk C, Abbott LF, and Ermentrout B (1994) *When inhibition not excitation synchronizes neural firing.* J. of Comput. Neurosci. 1:313-321

[29] Winfree A. T. (2001) *The Geometry of Biological Time,* 2nd edn. New York: Springer.

[30] Wang XJ, Buzsáki (1996) *Gamma oscillation by synaptic inhibition in a hippocampal interneuronal network model.* J. Neurosci. 16:6402-6413.

FIGURE LEGENDS

Figure 1. Network activity states at different values of coupling strength, $\bar{g}_{syn}$. The potentials of the two cells are shown as red and black traces, respectively. (a) Synchronous phase-locked firing ($\bar{g}_{syn} = 0.03$). The spiking period is close to the unperturbed period of 45 ms. (b) Alternating-order (leap-frog) spiking ($\bar{g}_{syn} = 0.17$) (c) Period-2 alternating-order spiking ($\bar{g}_{syn} = 0.22$) (d) Chaotic state, irregular inter-spike intervals ($\bar{g}_{syn} = 0.29$) (e) Bursting (3:3 alternating-order firing, $\bar{g}_{syn} = 0.34$) (f) Spike-suppress state ("oscillator death", $\bar{g}_{syn} = 0.5$)

Figure 2. Bifurcation diagram of the Morris-Lecar model network. ISI_∞, the asymptotic values of the intervals between consecutive spikes (not necessarily spikes of the same cell) are plotted as a function of the coupling strength, $\bar{g}_{syn}$, for two values of synaptic decay time: (a) $\tau_{syn} = 1$ and (b) $\tau_{syn} = 2$. The dotted lines correspond to each of the six activity states in Figure 1(a)-(f). Note the difference in scale along the $\bar{g}_{syn}$ axis

Figure 3. Effect of an increase in coupling strength on the stability of phase-locked firing in an excitatory network (a) and an inhibitory network (b). $\bar{g}_{syn}$ changes from 0.01 to 0.2 in both cases. In the case of excitation (a), anti-phase synchronous firing is stable for a wide range of coupling strength, while the phase-locked synchronous firing is readily destabilized in the case of mutual inhibition (b)

Figure 4. Effect of non-weak coupling on the phase-plane trajectory of the postsynaptic cell. Double arrows indicate the movement of the V-nullcline during each cycle of the network oscillation. (a) In the case of excitation, an increase in synaptic coupling causes no qualitative change in the phase plane geometry. (b) For sufficiently strong inhibition, the V-nullcline of the post-synaptic cell intersects the w-nullcline with each presynaptic input, pushing the cell below the excitation threshold and off the limit cycle trajectory. Thick blue curve indicates the trajectory of each cell during one cycle of the alternating-order spiking shown in Fig. 1(b),(c)

Figure 5. Phase plane dynamics of the two coupled cells during periodic leap-frog alternating-order spiking (top left trace). The tadpole-shaped curves schematically represents the phase plane trajectory in Figure 4(b). The sequence of five panels describe the phase-plane dynamics underlying the spike sequence shown in top left panel: (i) "red" cell spikes; (ii) "blue" cell spikes, lowering the nullcline of the red cell, and trapping it in the passive phase of the trajectory (tadpole tail); (iii) termination of the blue cell's spike; red cell gradually recovers from inhibition; (iv) blue cell bypasses the red cell 1 along the unperturbed limit cycle trajectory; (v) blue cell spikes again, followed by the spike of the red cell. The process then repeats itself, with red cell emitting the next spike

Figure 6. Reduced phase description of the alternating-order state. (a) In the model with continuous synaptic interaction, the alternating-order spiking is a continuous trajectory on the 2-torus. The spike times of the two cells correspond to the intersections of the trajectory with the $\phi_1 = 1$ and the $\phi_2 = 1$ boundaries, respectively. The change in spiking order requires the trajectory to self-intersect. The dashed gray lines indicate the formal equivalence of the continuous coupling description to the pulse-coupled model description shown in (b). In (b), the spike of cell i ($\phi_i = 1$) causes a discontinuous drop (red arrow) in the phase of the partner cell j by amount $\Delta(\phi_j)$, where $\Delta(\phi)$ is the spike-time response characteristic of the cell (which we define to be positive in case of a phase delay). The change in firing order requires the phase domain to be extended to the passive negative value branch. In order for the spiking order to change, the value of the spike-time response $\Delta(\phi)$ should be greater than ϕ for one of the two spikes that each cell emits in one cycle of the oscillation.

Figure 7. Constructing the inter-spike phase return map for the periodic alternating-order spiking, $\phi_1 \to \phi_2 = \Phi(\phi_1)$. (a) In each cycle of the alternating-order spiking, one of the cells spikes twice (dashed red lines at times t_1 and t_2) between two spikes of the partner cell (black lines). The phase

variables ϕ_1 and ϕ_2 are inter-spike intervals normalized by the unperturbed period of each oscillator. Note that the phase difference between two red spikes equals 1 (the unperturbed period). The phase of the cell at the time of arrival of the second input is $1+\phi_1-\Delta(\phi_1)$, where $\Delta(\phi_1)$ is the phase delay due to the arrival of the first input. (b) Black curve represents the STRC of each ML oscillator, $\Delta(\phi)$, while the blue curve represents the return map $\Phi(\phi)$ (Eqs. 12). The synaptic coupling strength is $\bar{g}_{syn} = 0.09$

Figure 8. Phase-map analysis of the alternating-order spiking. (a) The cell potential time courses of the two coupled ML oscillators are shown in red and black, respectively, for $\bar{g}_{syn} = 0.2$. (b) Equilibrium inter-spike phase difference ($\phi = 0.144$) in the alternating-order state satisfies Eq. 5, which can be re-written as $\Delta(1-\psi) = \phi - \psi$ in terms of the quantity $\psi = 1 - \xi = \Delta(\phi) - \phi$. In this simulation, $\psi = \Delta(\phi) - \phi = 0.0468$, and $\Delta(1-\psi) = 0.095$. The stability condition is given by Eq. 9: $|[1-\Delta'(1-\psi)][\Delta'(\phi)-1]| < 1$. (c) Inter-spike phase sequence artificially generated (emulated) by the phase return map $\Phi(\phi)$ (Eqs. 4) using the simplified quadratic STRC shown in (d). (d) Quadratic spike-time response curve $\Delta(\phi) = 4m\phi(1-\phi)$, where $m = 0.5$ is the maximum phase resetting.

Figure 9. Comparison between the first- and the second-order spike-time response curves of the Morris-Lecar oscillator. The first-order STRC is shown in blue, while the second-order STRC is shown in red, for synaptic conductance of $\bar{g}_{syn} = 0.2$. The two functions satisfy the consistency (periodic boundary) condition $\Delta(0) = \Delta_2(1)$, where $\Delta(\cdot)$ and $\Delta_2(\cdot)$ are the first- and the second-order STRC, respectively. The second-order phase resetting provides only negligible contribution to the alternating-order firing (cf. Fig. 8(a)): $\Delta_2(\phi) = 0$; $\Delta_2(\eta) = 1.4 \cdot 10^{-4}$

Figure 10. Period-2 (unequal phase) alternating-order leap-frog spiking emulated using the quadratic STRC (a) Inter-spike phase sequence generated by the emulator is similar to the period-2 leap-frog spiking exhibited by the ML network, shown in Figure 1(c). The stable phase differences are $\phi_1 = 0.254$ and $\phi_2 = 0.463$. (b) The period-2 leap-frog existence conditions (Eqs. 13) are satisfied for the quadratic STRC $\Delta(\phi) = 4m\phi(1-\phi)$, where $m = 0.55$ is the peak phase resetting

Figure 11. Emulated bifurcation diagram for the inter-spike interval differences as a function of synaptic conductance for the quadratic STRC. Asymptotic inter-spike interval differences ISI_∞ are plotted as a function of the STRC peak amplitude, m

Figure 12. The network of three all-to-all coupled ML oscillators can exhibit splay states in a certain range of synaptic coupling strength ($\bar{g}_{syn} = 0.14$). The potentials of the three cells are shown as black, red, and blue traces. Note the change in spiking order: 1,2,3 $\rightarrow$ 3,2,1 $\rightarrow$ 1,2,3 $\rightarrow$ ...

APPENDIX

Derivation of the alternating-order phase map with second-order phase resetting

We will use the diagram in Fig. 7(a) to derive the map in the case of non-negligible second-order phase resetting, $\Delta_2(\phi)$. Let $\{\phi_n, \xi_n\}$ denote the two phases of the postsynaptic cell at the time of arrival of each of the two spikes in n-th period of the oscillation. In the case of zero second-order resetting, Fig. 7(a) illustrates the relationship between these phases, $\xi_n = 1 + \phi_n - \Delta(\phi_n)$. However, due to non-zero second-order phase resetting received by the presynaptic cell in the preceding cycle, $\Delta_2(\xi_{n-1})$ (where ξ_{n-1} is its phase at the time of arrival of the first black spike in Fig. 7(a)), the interval between two spikes of the presynaptic cell in the current cycle, denoted γ_n, will not be equal to 1:

$$\gamma_n = 1 + \Delta_2(\xi_{n-1}) > 1 \tag{14}$$

Therefore, the modified relationship between ξ_n and ϕ_n reads

$$\xi_n = \gamma_n + \phi_n - \Delta(\phi_n) \tag{15}$$

Note that we neglect the much smaller second-order phase-resetting due to the first spike of the presynaptic cell in each period of the 2:2 mode: $\Delta_2(\phi_n) << \Delta_2(\xi_n)$. Finally, given the phase ξ_n of the postsynaptic cell right before receiving its second input, one can easily find its first passage time, ϕ_{n+1} (i.e. interval ϕ_2 in Fig. 7(a)), using the first passage time condition

$$\xi_n - \Delta(\xi_n) + \phi_{n+1} = 1 \tag{16}$$

Solving this system of equations for ξ_n yields the map

$$\xi_{n+1} = 2 - \xi_n + \Delta(\xi_n) - \Delta(1 - \xi_n + \Delta(\xi_n)) + \Delta_2(\xi_n) \tag{17}$$

which can be re-written in a more compact form as

$$\xi_{n+1} = 1 + \phi_n - \Delta(\phi_n) + \Delta_2(\xi_n) \tag{18}$$

If we substitute the conditions for synchronous firing, $\xi_n = 1$, $\phi_n = 0$, we obtain $\Delta_2(1) = \Delta(0)$, which is the correct periodicity condition relating the first- and second-order STRC curves. Therefore, the synchronous solution is always a fixed point of Eq. 17.

Differentiating Eq. 17 yields the stability condition

$$|[1 - \Delta'(\xi)][\Delta'(\phi) - 1] + \Delta_2'(\xi)| < 1 \tag{19}$$

which agrees with Eq. 9 when $\Delta_2(\cdot)$=0. Close to the bifurcation from synchrony to leap-frog spiking, $\xi \approx 1$, $\Delta'(\xi) \approx 0$, and therefore

$$|\Delta'(\phi) + \Delta_2'(\xi) - 1| < 1$$

which yields

$$0 < \Delta'(\phi) + \Delta_2'(\xi) < 2 \tag{20}$$

Recall that $\phi = 1 - \xi + \Delta(\xi)$ (Eq. 16). A more general stability condition for the case of non-negligible $\Delta_2(\phi_n)$ is given by Maran and Canavier (2007).

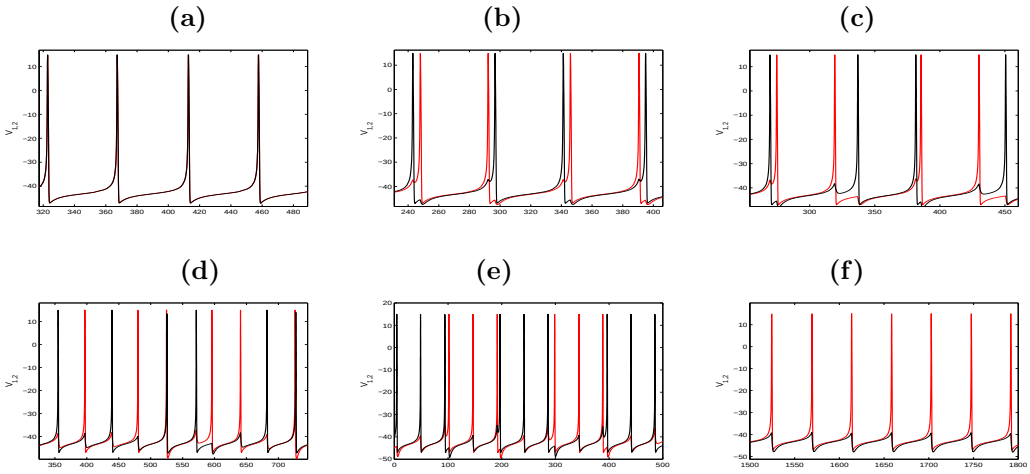

Figure 1.

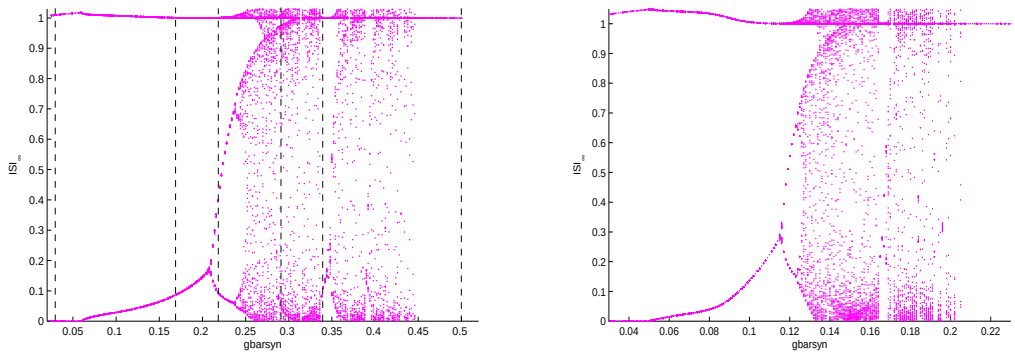

(a) $\tau_{syn} = 1$ **(b)** $\tau_{syn} = 2$

Figure 2.

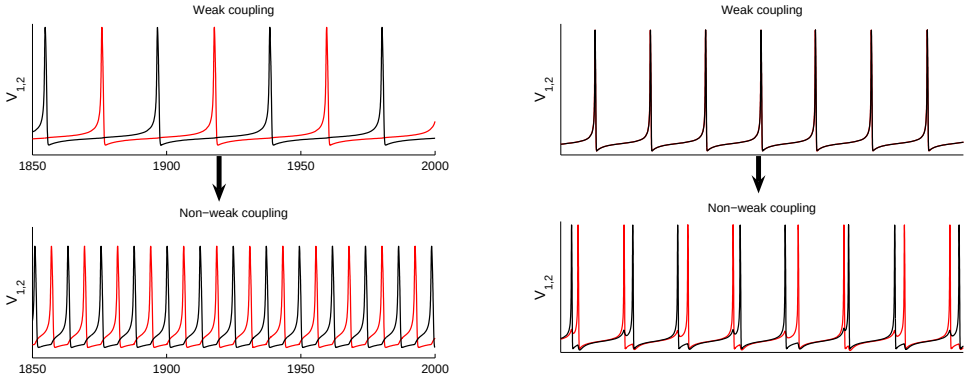
Weak coupling
V1,2
1850
1900
1950
2000
Non−weak coupling
V1,2
1850
1900
1950
2000
Weak coupling
V1,2
Non−weak coupling
V1,2

(a) **(b)**

Figure 3

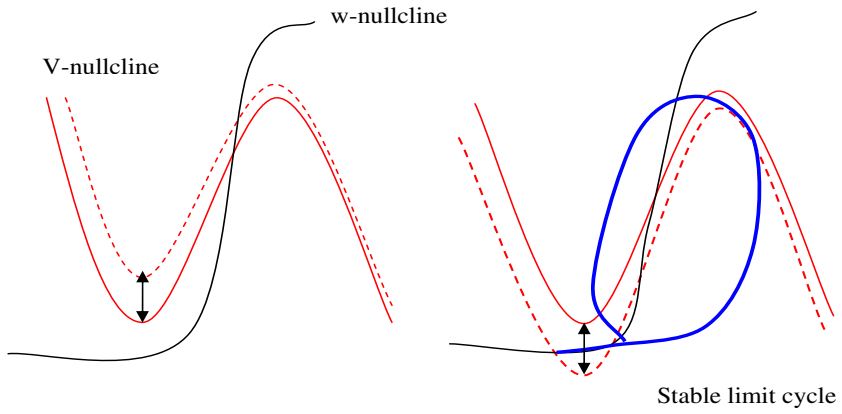

(a) (b)

Figure 4.

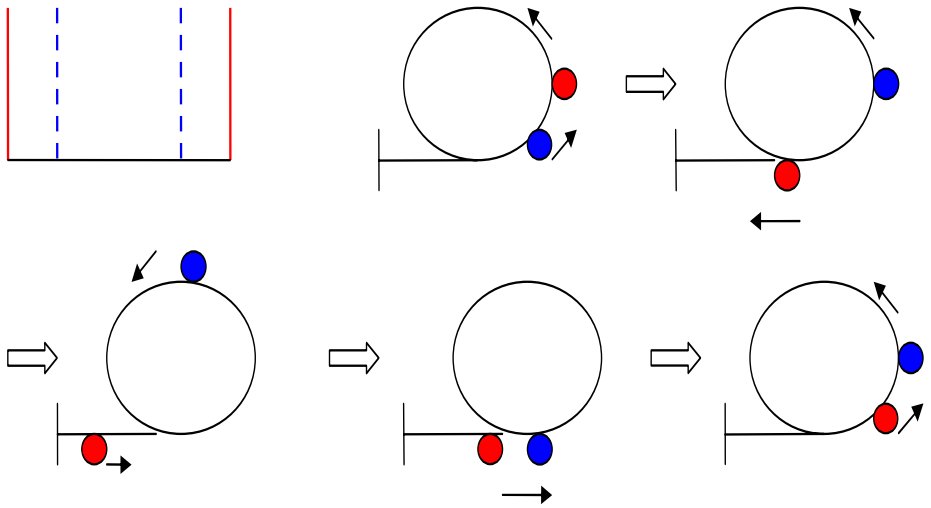

Figure 5.

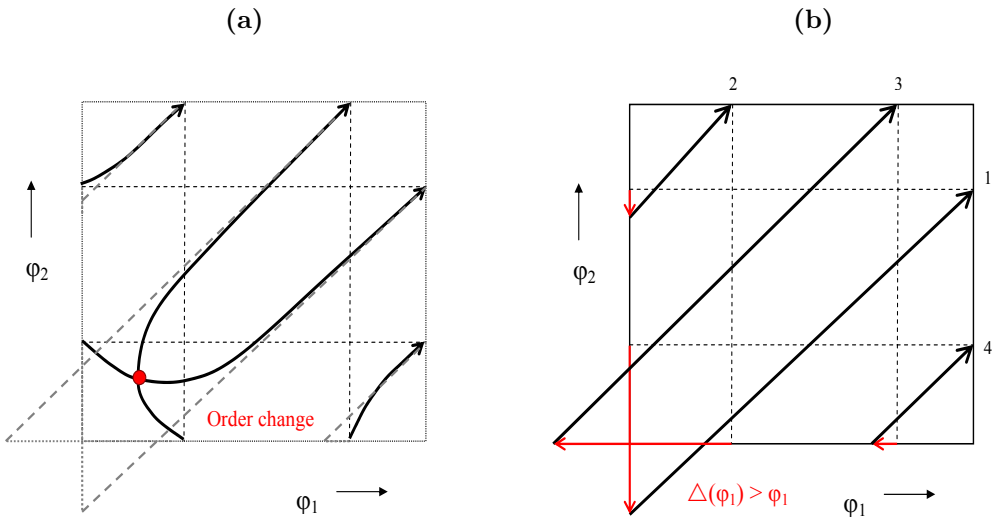

Figure 6.

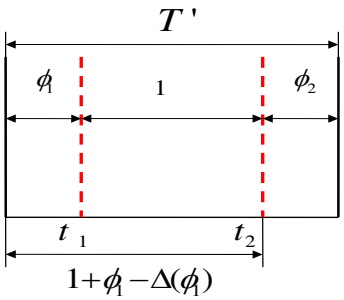
T '
ϕ_1
1
ϕ_2
t_1
t_2
$1+\phi_1-\Delta(\phi_1)$

(a)

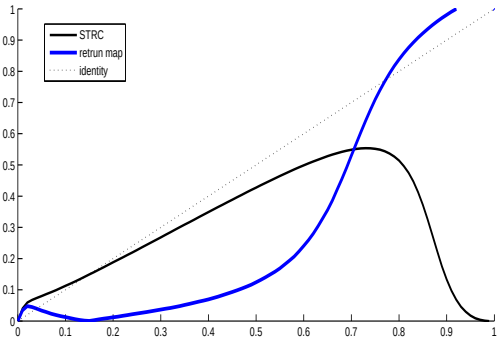
STRC
retrun map
identity
0
0.1
0.2
0.3
0.4
0.5
0.6
0.7
0.8
0.9
1

(b)

Figure 7.

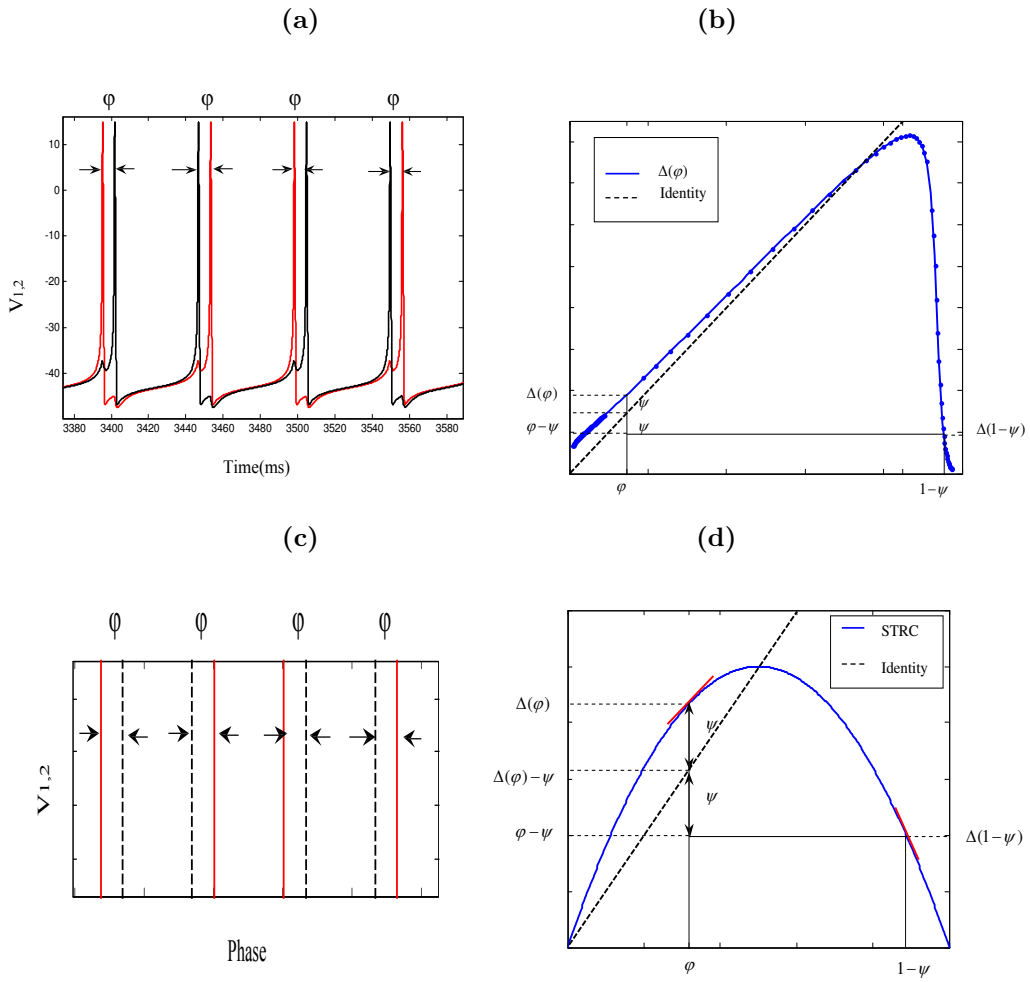

Figure 8.

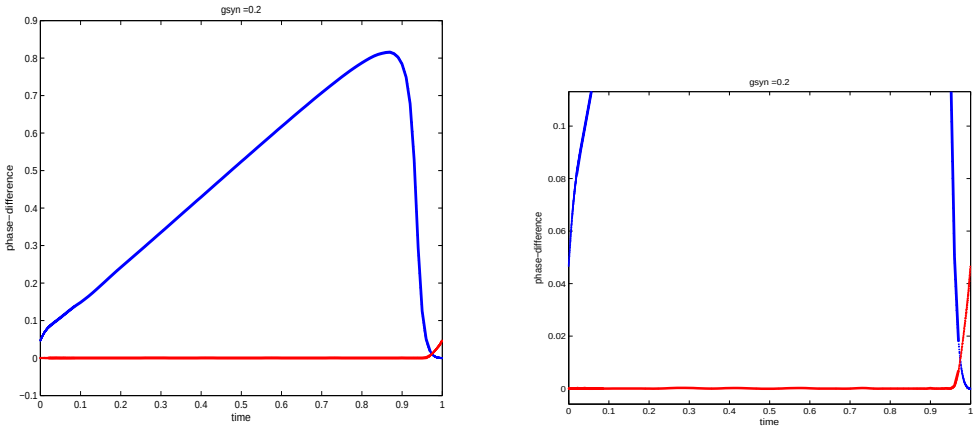
gsyn =0.2
phase−difference
time
gsyn =0.2
phase−difference
time

(a) **(b)**

Figure 9.

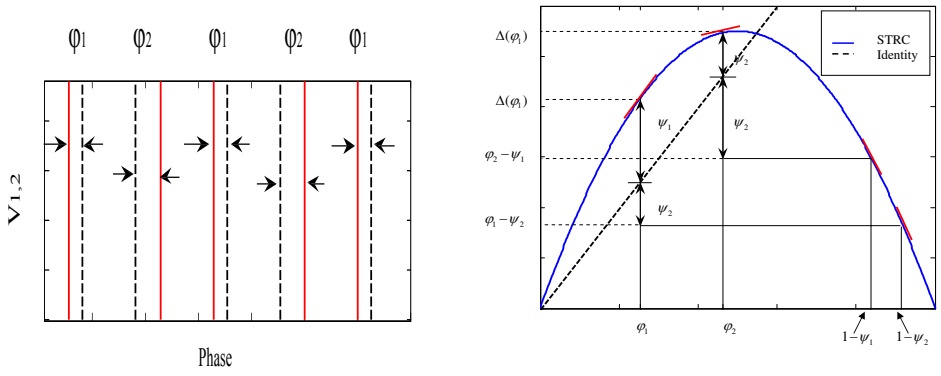
φ1
φ2
φ1
φ2
φ1
V1,2
Phase
Δ(φ1)
Δ(φ1)
φ2 − ψ1
φ1 − ψ2
ψ2
ψ1
ψ2
ψ2
φ1
φ2
1−ψ1
1−ψ2
STRC
Identity

(a) **(b)**

Figure 10.

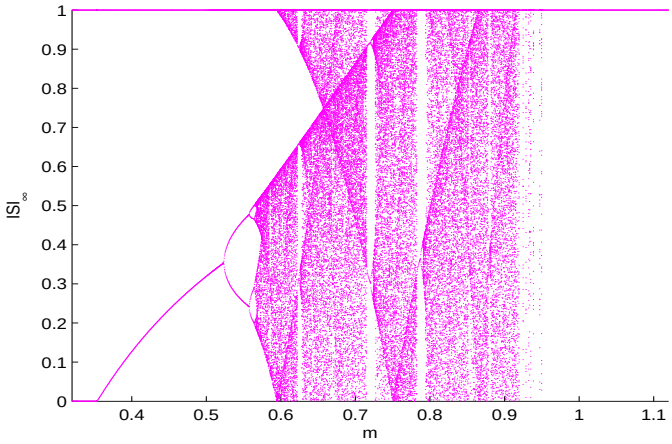

Figure 11.

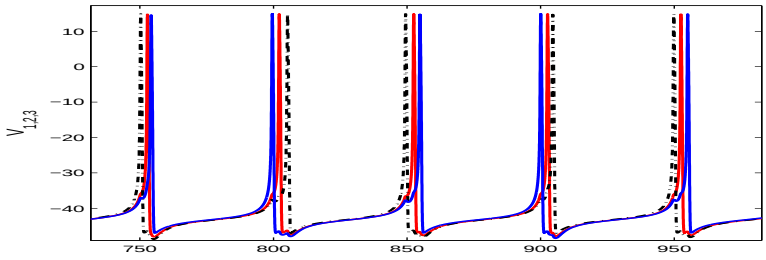

Figure 12.